Enhanced peroxidase-like properties of Au@Pt DNs/NG/Cu^{2+} and application of sandwich-type electrochemical immunosensor for highly sensitive detection of CEA

Hui Lv, Yueyun Li, Xiaobo Zhang, Zengqiang Gao, Chunyan Zhang, Shuan Zhang, Yunhui Dong

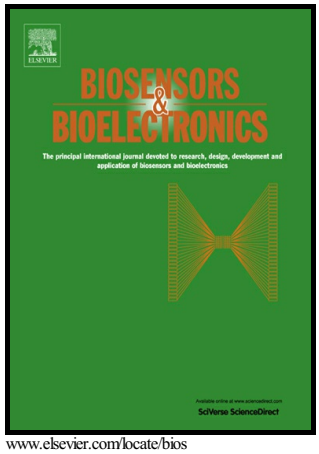

www.elsevier.com/locate/bios

PII: S0956-5663(18)30286-0
DOI: https://doi.org/10.1016/j.bios.2018.04.025
Reference: BIOS10421

To appear in: *Biosensors and Bioelectronic*

Received date: 5 February 2018
Revised date: 21 March 2018
Accepted date: 13 April 2018

Cite this article as: Hui Lv, Yueyun Li, Xiaobo Zhang, Zengqiang Gao, Chunyan Zhang, Shuan Zhang and Yunhui Dong, Enhanced peroxidase-like properties of Au@Pt DNs/NG/Cu^{2+} and application of sandwich-type electrochemical immunosensor for highly sensitive detection of CEA, *Biosensors and Bioelectronic,* https://doi.org/10.1016/j.bios.2018.04.025

Enhanced peroxidase-like properties of Au@Pt DNs/NG/Cu^{2+} and application of sandwich-type electrochemical immunosensor for highly sensitive detection of CEA

Hui Lv[a], Yueyun Li[a,*], Xiaobo Zhang[a], Zengqiang Gao[a], Chunyan Zhang[a], Shuan Zhang[a], Yunhui Dong[a]

School of Chemistry and Chemical Engineering, Shandong University of Technology, Zibo 255049, P.R. China

*Corresponding author. Tel: +86-533-2781203; Fax: +86-533-2781664.

E-mail address: liyueyun71@163.com

Abstract

Effective treatment of cancer depends upon the early detection of the tumor marker. Here, we report on the development of a new immunosensor for early detection of carcinoembryonic antigen (CEA). Cubic Au@Pt dendritic nanomaterials functionalized nitrogen-doped graphene loaded with copper ion (Au@Pt DNs/NG/Cu^{2+}) with enhanced peroxidase-like properties was synthesized as labels to effectively capture and immobilize secondary anti-CEA. The Au@Pt DNs with more active surface area could efficiently enhance electrocatalysis for reduction of hydrogen peroxide (H_2O_2). Meanwhile, with good conductivity and large specific surface area, NG can immobilize a large amount of Au@Pt DNs. Furthermore, after adsorbed Cu^{2+} can further promote the redox of H_2O_2 and amplify the signal of the immunosensor. For the immobilization of primary antibodies, Au nanoparticles functionalized polydopamine (Au@PDA) were used as transducing materials to modify glassy carbon electrodes and enhance the electron transfer efficiently. Under optimal conditions, the immunosensor exhibited a satisfactory response to CEA with a limit detection of 0.167 pg/mL and linear detection range from 0.5 pg/mL to 50 ng/mL. Based on the high sensitivity and specificity of the immunosensor, we propose this multiple amplified biosensor for early detection of CEA.

Keywords: Sandwich-type electrochemical immunosensor; Cubic

Au@Pt dendritic nanomaterials; Nitrogen-doped graphene; Au nanoparticles functionalized polydopamine; Carcinoembryonic antigen.

1. Introduction

Carcinoembryonic antigen (CEA) as one of the most broad-spectrum tumor markers, is a surface-expressed tumour-associated antigen, and it produced abundantly in essentially all human colon carcinomas and in a high proportion of carcinomas at many other sites (Li et al. 2016; Zbar et al. 1998). Normally, the CEA level greater than 5 ng/mL will usually trigger a workup to look for possible disease recurrence (Barton et al. 2014). Consequently, the sensitive and early determination of CEA plays a key role in the prognosis of the original carcinoma and clinical tumor diagnoses (Hasanzadeh et al. 2016). In the last few decades, lots of methods have been used to analyze CEA in human serum, including enzyme-linked immunosorbent assay (Li et al. 2010), capillary electrophoresis-chemiluminescence (Liu et al. 2009), fluorescence (Chen et al. 2016), and so forth. Nonetheless, methods with higher sensitivity and better selectivity for the quick and quantitative detection of CEA are still urgently demanded.

Until now, electrochemical methods with low cost, simple instrumentation and high selectivity have aroused widespread concerns in the fields of food safety control (Guo et al. 2017), environmental pollutant monitoring (Wen et al. 2016), clinical analysis and diagnosis of cancers (Wang et al. 2017a). Electrochemical immunosensor based on the remarkable sensitivity and selectivity of specific interaction between an

antibody and its corresponding antigen (Sheng et al. 2017). Due to immune proteins are not intrinsically able to act as redox partners in an immunoassay reaction, most immunoreactions use secondary antibodies (Ab_2) conjugated with different signal amplification labels to monitor the current response from the addition of redox molecules (i.e., H_2O_2) (Li et al. 2017; Zhang et al. 2018). Therefore, it is meaningful to prepare an effective material with good catalytic performance to construct a highly sensitive immunosensor. Graphene, emerging as a two-dimensional material, has shown its fascinating applications in biosensing (Fan et al. 2012). More interestingly, nitrogen is considered as an excellent element to dope graphene, synthesizing nitrogen-doped graphene (NG) possessed a much larger surface area, better electrical conductivity, and further enhanced electrocatalytic activity toward H_2O_2 reduction compares with graphene (Wang et al. 2010; Yadav and Dixit, 2017; Yang et al. 2016). Therefore, synthesizing NG-based nanocomposites with excellent catalytic activity is crucial for improving the sensitivity and stability of electrochemical immunosensors.

Recently, gold (Au) based bimetallic core-shell nanomaterials with good biocompatibility, excellent conductivity and high catalytic ability have been reported to functionalize NG for biosensing applications (Wang and Yamauchi, 2011; Yang et al. 2015). It is well known that catalysis reaction is usually occurred on the catalyst surface, the shape

and composition of core and shell are strongly determined the properties of core-shell nanomaterials (Liu et al. 2016). Cubic nanoparticles (NPs) exposed more active sites compare to sphere NPs, leading to the enhancement of electrocatalytic efficiency (Sun and Xia, 2002). In this study, cubic gold@platinum dendritic nanomaterials (Au@Pt DNs) was synthesized to increase the sensitive of the immunosensor. Pt NPs with dendritic shape not only maximize Pt utilization efficiency (Lv et al. 2017; Wang and Yamauchi, 2010), but also expose abundant active sites to catalyze the reduction of H_2O_2 (Lim et al. 2008). In this consideration, the combination of Au@Pt DNs with NG to form a new nanomaterial (Au@Pt DNs/NG) exhibited excellent performance. On the one hand, Au@Pt DNs/NG was able to act as a carrier to immobilize antibodies owing to the stable Au-N and Pt-N bond between Au@Pt DNs and -NH_2 on antibodies (Jiang et al. 2015); on the other hand, it has a large surface area and exceptional adsorption capability to capture the copper ions (Cu^{2+}). The adsorbed Cu^{2+} can further promote the redox of H_2O_2 and be used to amplify the detection signal (Li et al. 2015). The resultant Au@Pt DNs/NG/Cu^{2+} with enhanced peroxidase-like properties, can improve the detection sensitivity of the immunosensor.

In this work, a sandwich-type electrochemical immunosensor based on a new signal amplification strategy was prepared for the detection of CEA. Au NPs functionalized polydopamine (Au@PDA) was synthesized

and used as electrode substrate material, PDA molecules with a great amount of amino groups can form covalent bonds to capture a large number of the primary antibody (Ab_1), so as to increase the electrochemical performance (Zhang et al. 2016; Wang et al. 2017b). With the secondary antibody (Ab_2) adsorbed onto Pt and Au, the resulting Au@Pt DNs/NG/Cu^{2+}-Ab_2 were used as labels for the preparation of immunosensor, which demonstrated an enhanced peroxidase-like performance. The developed immunosensor exhibited wide linear range and low detection limit for CEA with high sensitivity, good reproducibility and stability, which may find wide potential application for ultrasensitive detection of different tumor markers in clinical analysis.

2. Experimental section

2.1. Materials and apparatus

CEA, CEA antibody (anti-CEA) and Human CEA ELISA Kit were purchased from Dingguo Biochemical Reagents (Beijing, China). The other details are provided in Supplementary material (SM).

2.2. Preparation of Au@PDA

The Au NPs was prepared according to a published method (Frens, 1973). The other details are provided in SM.

2.3. Synthesis of label material

The synthesis of the NG was carried out based on previous reports (Zhang et al. 2011). The Au@Pt DNs was synthesized by the method

described previously (Fan et al. 2008). The other details are provided in SM.

Au@Pt DNs/NG/Cu^{2+} was synthesized by a simple method. 10 mg of the prepared NG was dispersed in 20 mL of above synthesized Au@Pt DNs solution (1.0 mg/mL) under continuously sonicated for 2 hours. The black Au@Pt DNs/NG was obtained by centrifugation and dried in the vacuum oven at 35 °C. And then 10 mg of Au@Pt DNs/NG were dispersed in 10 mL ultrapure water, 1 mM $CuCl_2$ was added and kept stirring for 24 hours at room temperature. The resultant Au@Pt DNs/NG/Cu^{2+} were centrifuged and then dried at room temperature. The other details are given in SM.

2.4. Preparation of Au@Pt DNs/NG/Cu^{2+}-Ab_2

Au@Pt DNs/NG/Cu^{2+} (5.0 mg/mL, 1.0 mL) was mixed with the solution of secondary antibodies (Ab_2) (20 μg/mL, 1.0 mL) and oscillated at 4 °C for 6 hours. Subsequently, the dispersion was centrifuged and rinsed with PBS (pH = 7.0) to remove the unbound Ab_2. The sediment was re-dispersed in 1.0 mL of PBS (pH = 7.0) and stored at 4 °C. Fig. 1A shows the preparation procedure of Au@Pt DNs/NG/Cu^{2+}-Ab_2.

2.5. Fabrication of the immunosensor

The schematic diagram of the stepwise self-assembly procedure of the proposed immunosensor is shown in Fig. 1B. First, the bare glassy carbon electrode (GCE) was polished with 0.3 and 0.05 μm alumina

powder, and cleaned thoroughly with ultrapure water. Then, 6.0 μL Au@PDA (2.0 mg/mL) was casted and dried in air. Following that, 6.0 μL Ab_1 (10 μg/mL) was incubated and dried at 4 °C. After washing, 3.0 μL BSA solution (1.0 wt%) was incubated onto the electrode for 1 hour to block nonspecific binding sites. After rinsed with PBS buffer, different concentrations of CEA were incubated to ensure the specific binding between CEA and Ab_1. Finally, 6.0 μL prepared Au@Pt DNs/NG/Cu^{2+}-Ab_2 (2.5 mg/mL) was dropped onto the surface of electrode for 40 min. The prepared electrodes were washed with PBS and stored at 4 °C for further use.

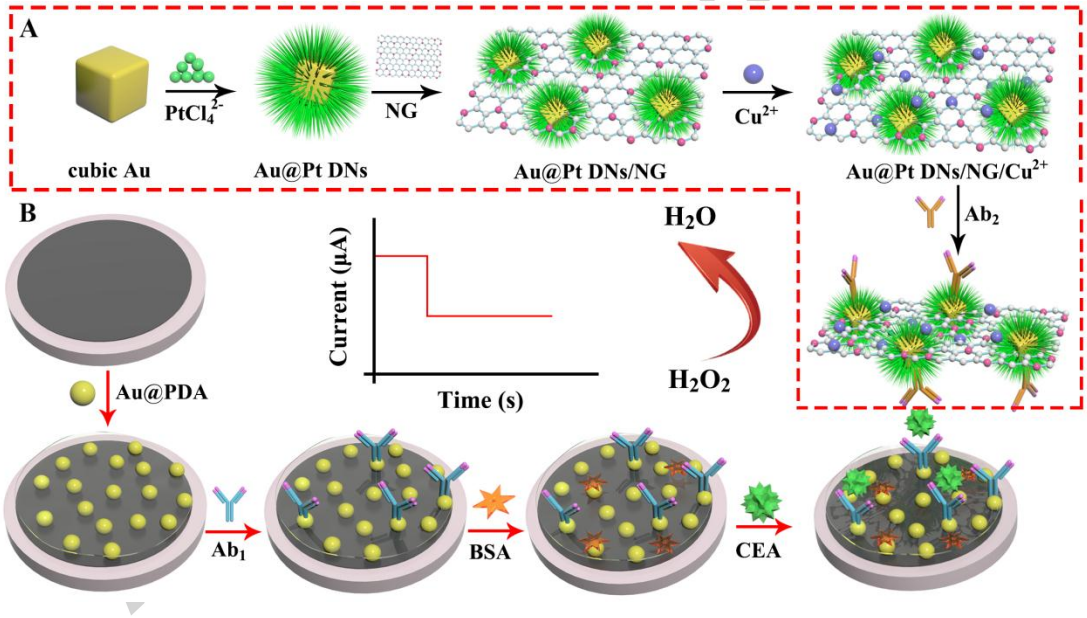

Fig. 1. (A) The preparation procedures of Au@Pt DNs/NG/Cu^{2+}-Ab_2. (B) The fabrication process of the sandwich-type electrochemical immunosensor.

2.6. Detection of CEA

The PBS (pH = 6.8) was used for all the electrochemical measurements. As shown in Fig. S1, -0.4 V was chose as scanning

potential for amperometric *i-t* measurement of the electrochemical immunosensor in order to reduce the background current and minimize the responses of common interference ingredient. After the background current was stabilized, 10 μL, 5 mol/L H_2O_2 was added to 10 mL PBS and the current change was recorded.

3. Results and discussion

3.1. Characterization of Au@PDA

TEM image of the Au NPs was shown in Fig. 2A. It can be found that the obtained Au NPs had formed uniform globular morphology with an average size of 13 nm. Fig. 2B showed the TEM image of Au@PDA with a core-shell structure, a layer PDA coating of 5 nm in thickness surrounding the Au NPs. In addition, Au@PDA modified bare GCE in the same sweep speed (50 mV/s) continuous sweep 40 times by CV (Fig. 2D), we observed no obvious change of the peak current and peak potential. Therefore, it clearly confirmed that Au@PDA has good stability.

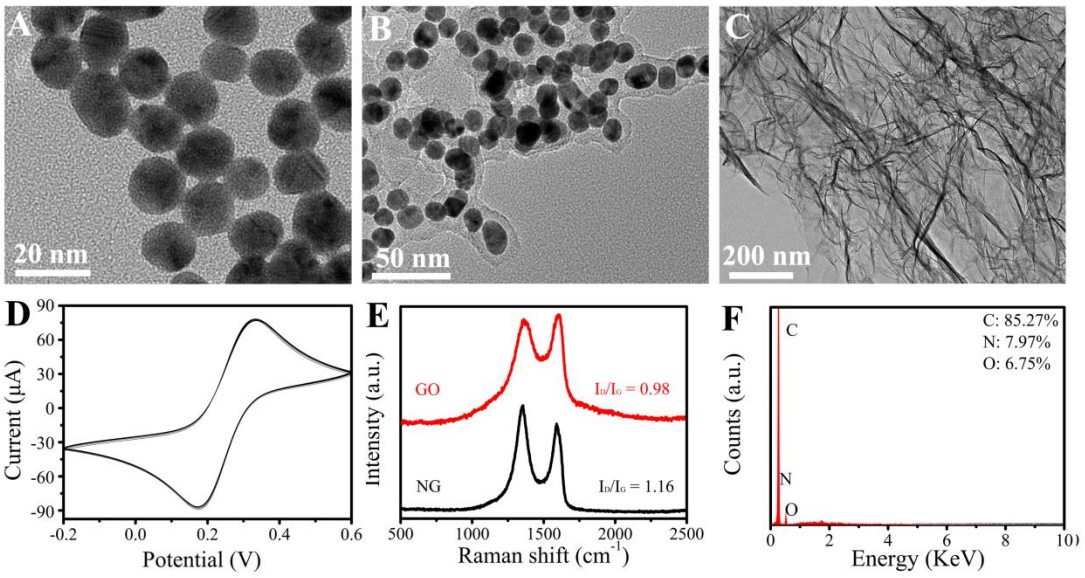

Fig. 2. TEM image of (A) Au NPs, (B) Au@PDA, (C) NG. (D) CV of Au@PDA modified bare GCE (sweep speed: 50 mV/s). (E) Raman spectra of GO and NG. (F) EDX spectrum of NG.

3.2. Characterization of Au@Pt DNs/NG/Cu^{2+}

Fig. 2C showed the characterization of NG. From the TEM image, the NG with thin wrinkled paper-like structure was readily observed. Raman spectroscopy is a very useful method to characterize NG. Raman spectra of GO and NG were shown in Fig. 2E, the type D-band at 1350 cm^{-1} and G-band at 1590 cm^{-1} were observed from the resultant spectra of both GO and NG (Yadav and Dixit, 2017). I_D/I_G ratio in the Raman spectra was observed for the evaluation of the disorder in the carbon materials. I_D/I_G ratio in GO was 0.98, which increased to 1.16 for NG, indicating a higher distortion of the synthesized NG. EDX (Fig. 2F) result demonstrated the existence of nitrogen elements in graphene oxide (GO), implying the nitrogen elements have been successfully doped in the GO.

As shown in Fig. S2, the N_2 adsorption-desorption isotherm indicated the BET surface area of the NG was 93.8 m^2/g.

Fig. 3A-C showed the morphology of Au@Pt DNs. Fig. 3A showed the TEM image of cubic Au, it manifested that the obtained Au NPs had formed cubic morphology with an average size of 20 nm. The high-resolution TEM (HRTEM) image (inset in Fig. 3A) showed a well-defined faces with the interplanar spacing. TEM image of the Au@Pt DNs was shown in Fig. 3B, indicating Au@Pt DNs had formed highly uniform dendritic morphology with a regular size. From the HRTEM image (Fig. 3C), it further revealed the morphology of the Au@Pt DNs, each nanocrystal had a cubic core surrounded by a dendritic shell. Meanwhile, images obtained by the elemental mapping patterns (Fig. S3A-B) and the line-scanning data (Fig. S3C) of Au@Pt DNs, displaying the center of the material is cubic Au, whereas Pt as dendritic at the outer edge.

Fig. 3D showed the SEM of Au@Pt DNs/NG. Clearly, Au@Pt DNs were connected to the NG. Besides, EDX spectrum (Fig. S4) of Au@Pt DNs/NG confirmed that the presence of the C, N, O, Pt and Au elements, which demonstrated the Au@Pt DNs had been loaded on the surface of NG.

Electrochemical characteristic of Au@Pt DNs/NG/Cu^{2+} was investigated by dropping the suspension of the nanomaterial on a clean

GCE, and then tested by CV (Fig. 3E) and amperometric *i-t* (Fig. 3F). As shown in Fig. 3E, the NG (curve a) displayed a lower redox peak current than Au@Pt DNs (curve b). Furthermore, both the anodic and cathodic peak currents at Au@Pt DNs/NG/GCE (curve c) showed a dramatic increase, reflecting that more Au@Pt DNs were attached on the electrode surface by loading on the NG. After the process of adsorbing the Cu^{2+}, the redox peak current of the Au@Pt DNs/NG/Cu^{2+} (curve d) further increased, indicating the Cu^{2+} had been successfully adsorbed by Au@Pt DNs/NG and can further enhance the electrical conductivity. The conclusion drew by amperometric *i-t* accordance with the result of CV. As illustrated in Fig. 3F, a teeny current response was detected when the NG (curve a) was coated onto the electrode, which indicated that the low catalytic activity of the NG. When Au@Pt DNs was alone coated onto the surface of the electrode, there was an obvious current response which due to the good catalytic capability of the Au@Pt DNs. Obviously, the current response of Au@Pt DNs/NG (curve c) was much larger than its single component. After the process of adsorbing the Cu^{2+}, the current response of Au@Pt DNs/NG/Cu^{2+} (curve d) can further increase. The results showed that the excellent catalytic capability and effective conductivity of Au@Pt DNs/NG/Cu^{2+}, indicating the successful synthesis of Au@Pt DNs/NG/Cu^{2+}.

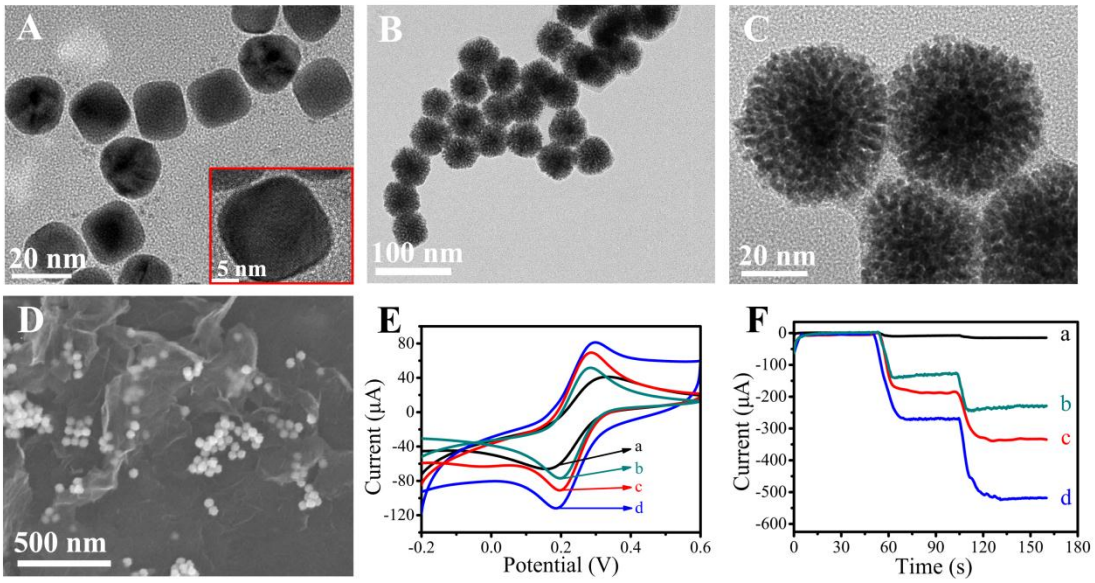

Fig. 3. (A) TEM and HRTEM (inset) image of cubic Au. (B) TEM image of Au@Pt DNs. (C) HRTEM image of Au@Pt DNs. (D) SEM image of Au@Pt DNs/NG. (E) CV of (a) NG, (b) Au@Pt DNs, (c) Au@Pt DNs/NG, (d) Au@Pt DNs/NG/Cu^{2+}. (F) amperometric i-t of (a) NG, (b) Au@Pt DNs, (c) Au@Pt DNs/NG, (d) Au@Pt DNs/NG/Cu^{2+}.

3.3. Characterization of Au@Pt DNs/NG/Cu^{2+} labels

In order to prove the successful immobilization of Ab_2 onto Au@Pt DNs/NG/Cu^{2+}, the Au@Pt DNs/NG/Cu^{2+}-Ab_2 was characterized using UV-vis spectroscopy (Fig. S5). According to the UV-vis spectral analysis, pure Ab_2 solution had a small peak at 285 nm (curve a). An obvious absorption peak was observed for Au@Pt DNs/NG/Cu^{2+} (curve b). When Au@Pt DNs/NG/Cu^{2+} was incubated with the Ab_2, an absorption peak around 285 nm was also observed (curve c), indicating the successful synthesis of Au@Pt DNs/NG/Cu^{2+}-Ab_2.

To demonstrate the significance of Au@Pt DNs/NG/Cu^{2+} as the

catalytic labels of Ab_2 for the signal amplification in the prepared immunosensor, different signal labels including NG (curve b), Au@Pt DNs (curve c), Au@Pt DNs/NG (curve d) and Au@Pt DNs/NG/Cu^{2+} (curve e) were used for designing the immunosensor (Fig. 4A). As shown in curve a, no obvious current response of the immunosensor without Ab_2 labeled probe, indicating the background current response cannot affect the precision of the immunosensor. Compared with others, the immunosensor using Au@Pt DNs/NG/Cu^{2+}-Ab_2 as labels displayed the highest current change. Therefore, Au@Pt DNs/NG/Cu^{2+} is an excellent labels for fabricating the proposed sandwich-type immunosensor.

3.4. Characterization of the immunosensor fabrication

As an effective technique for interfacial investigation, CV was harnessed to characterize the fabrication of the immunosensor. Fig. 4B showed the CV was performed in the solution containing 5.0 mM $K_3[Fe(CN)_6]$ and 0.1 M KCl by scanning the potential from -0.2 V to 0.6 V and the scan rate was 50 mV/s. As illustrated, Au@PDA (curve b) was modified on a bare GCE (curve a), the redox peak current was obviously increased due to the good conductivity of Au NPs. Then as Ab_1 (curve c), BSA (curve d), CEA (curve e) were modified onto the electrode surface, the redox peak current decreased gradually, because of the biologically active substances hindered the efficiency of electron transfer. Lastly, Au@Pt DNs/NG/Cu^{2+}-Ab_2 (curve f) was incubated, which displayed an

increased current response. Clearly, the assembly of electrochemical immunosensor was successful.

Electrochemical impedance spectroscopy (EIS) measurement was also employed to confirm the construction of sensing interface. The Nyquist plots of EIS were recorded from 0.1 to 10^5 Hz at 0.26 V in a solution containing 0.1 M KCl and 5.0 mM $[Fe(CN)_6]^{3-/4-}$. Inset in Fig. 4C illustrated the Randles equivalent circuit, which included the resistance of solution (R_s), the charge transfer resistance (R_{ct}), the double layer capacitance (C_{dl}), and the Warburg impedance (Z_w). The fitted values were obtained using ZSimpWin software and the relevant data were shown in Table S1. As shown in Fig. 4C, when coated with Au@PDA (curve b), the electrode showed a smaller semicircle than that of bare GCE (curve a), suggesting the Au@PDA nanocomposites with good conductivity can improve the electron transfer rate. However, the R_{ct} was increased gradually after successive assembly of Ab_1 (curve c), BSA (curve d), CEA (curve e) bioconjugate onto the electrode, which was attributed to the protein film reduces the electron transfer. However, when Au@Pt DNs/NG/Cu^{2+}-Ab_2 (curve f) was immobilized onto the surface of electrode, the R_{ct} was significantly decreased, due to the excellent conductivity of Au@Pt DNs/NG/Cu^{2+}-Ab_2. Therefore, both of the CV and EIS can demonstrate that the immunosensor was fabricated successfully.

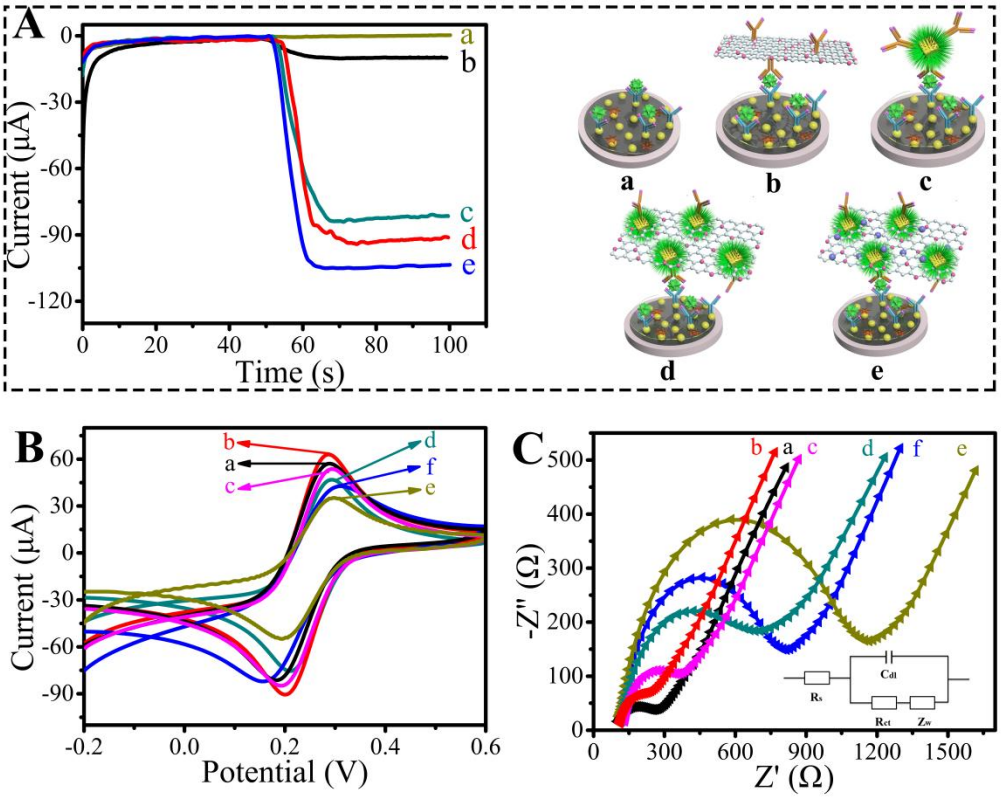

Fig. 4. (A) The current responses of immunosensor for the detection of 1 ng/mL of CEA with different signal labels including (a) without label, (b) NG, (c) Au@Pt DNs, (d) Au@Pt DNs/NG, (e) Au@Pt DNs/NG/Cu^{2+}. (B) CV of (a) GCE, (b) Au@PDA/GCE, (c) Ab_1/Au@PDA/GCE, (d) BSA/Ab_1/Au@PDA/GCE, (e) CEA/BSA/Ab_1/Au@PDA/GCE, (f) Au@Pt DNs/NG/Cu^{2+}-Ab_2/CEA/BSA/Ab_1/Au@PDA/GCE (potential from -0.2 V to 0.6 V and scan rate is 50 mV/s). (C) EIS of (a) GCE, (b) Au@PDA/GCE, (c) Ab_1/Au@PDA/GCE, (d) BSA/Ab_1/Au@PDA/GCE, (e) CEA/BSA/Ab_1/Au@PDA/GCE, (f) Au@Pt DNs/NG/Cu^{2+}-Ab_2/CEA/BSA/Ab_1/Au@PDA/GCE (frequency range from 0.1 Hz to 10^5 Hz and applied potential is 0.26 V). The inset in (C) is Randles equivalent circuit for EIS.

3.5. Optimization of the experimental conditions

In order to improve the sensitivity and analyze efficiency of the constructed immunosensor, the optimal concentration of Au@Pt DNs/NG/Cu^{2+}-Ab_2 was investigated. Fig. S6A showed that the current response increased with the variation of concentration from 0.5 mg/mL to 2.5 mg/mL, and then decreased with an increasing concentration from 2.5 mg/mL to 4.0 mg/mL. The current variations declared that the appropriate concentration of Au@Pt DNs/NG/Cu^{2+}-Ab_2 not only ensures the successfully specific binding between antigen and antibody but also efficiently enhances the catalytic performance; however, in high concentration, the excessively thick film of Au@Pt DNs/NG/Cu^{2+}-Ab_2 could hinder the electron transfer because of the increased interface resistance. Meanwhile, the concentration of Au@PDA is another important parameter for the performance of immunosensor. As seen in Fig. S6B, the current response is rapidly increased with the increasing concentration from 0.5 mg/mL to 2.0 mg/mL, and then the current change has decreased when the concentration becomes higher than 2.0 mg/mL, the increasing film thickness of Au@PDA may lead to an increase of interface electron transfer resistance. Thereby, the concentration of Au@Pt DNs/NG/Cu^{2+}-Ab_2 is 2.5 mg/mL and Au@PDA is 2.0 mg/mL were chosen as the optimizing concentration for this study.

The pH value of the detection solution is an important factor of

electrochemical behavior. The effects of solution pH on the current responses to CEA were shown in Fig. S6C. The current responses increased with increasing pH values from 5.8 to 6.8 and then decreased when the pH was over 6.8. Thus, PBS at pH 6.8 was selected for preparation of the detection solution. Furthermore, the incubation time is a great influence on the combination of antigen and antibody. As illustrated in Fig. S6D, the signal augmented with the passage of incubation time, and nearly became a constant value at 40 min. Hence, 40 min was chosen as the optimal incubation time.

3.6. Analysis and detection

Under the optimal conditions, the sandwich-type immunosensor using Au@Pt DNs/NG/Cu^{2+} as labels and Au@PDA as transducing materials were used to detect different concentrations of CEA. The current change was mainly due to the interaction between the labels of Au@Pt DNs/NG/Cu^{2+} and the substrate of H_2O_2, and the current responses toward CEA concentrations were shown in Fig. 5A. It can be obviously found that the current of the immunosensor increased proportionally with the increasing of CEA concentration. Moreover, when the as-prepared immunosensor was incubated with 0 ng/mL of CEA, a very low current response (Fig. 5A, a) was observed, implying that the effect of nonspecific adsorption on the proposed immunosensor can be ignored. Fig. 5B showed a linear relationship related to the logarithmic

values of CEA concentration from 0.5 pg/mL to 50 ng/mL with a low detection limit of 0.167 pg/mL (signal-to-noise ratio of 3). The regression equation of the calibration curve is: I = 104.96 + 17.9 lg$C$, with correlation coefficient of 0.9964.

The comparison of the linear range and detection limit between the proposed immunosensor and some published studies was listed in Table S2, which also illustrated that the designed immunosensor has a lower detection limit than some previously reported methods. The sensitivity was ascribed to several factors. Firstly, the application of NG as a support for catalysts is attractive because NG has useful properties, such as high electronic conductivity and surface area. Secondly, Au@Pt DNs as a novel material can provide higher specific surface areas and more exposed active sites, exhibiting excellent electrocatalytic activity to the reduction current of H_2O_2. Furthermore, Cu^{2+} was absorbed in Au@Pt DNs/NG can further promote the redox of H_2O_2 using the synergetic effect.

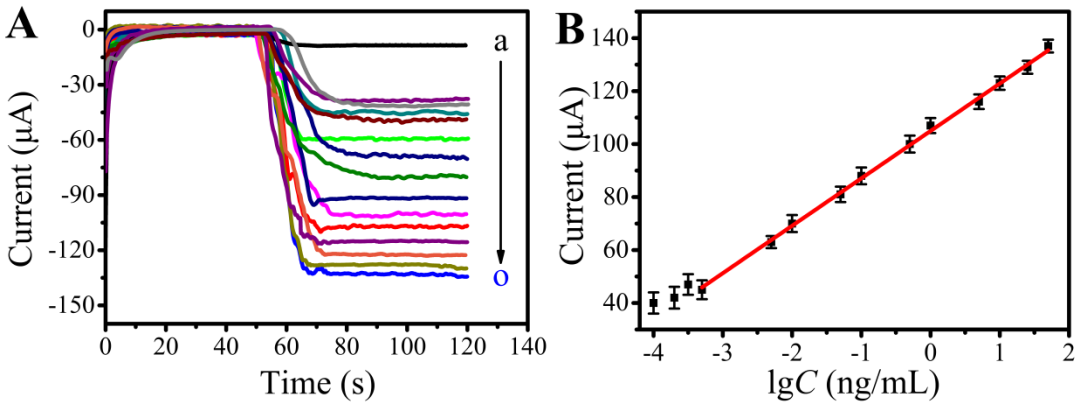

Fig. 5. (A) Current response of the immunosensor to different concentrations of CEA,

(a) 0 ng/mL, (b) 100 fg/mL, (c) 200 fg/mL, (d) 500 fg/mL, (e) 300 fg/mL, (f) 5.0 pg/mL, (g) 10 pg/mL, (h) 50 pg/mL, (i) 100 pg/mL, (j) 500 pg/mL, (k) 1.0 ng/mL, (l) 5.0 ng/mL, (m) 10 ng/mL, (n) 25 ng/mL, (o) 50 ng/mL. (B) Calibration curves of the immunosensor to different concentrations of CEA. Error bar = RSD (n = 5).

3.7. Reproducibility, selectivity, and stability of the immunosensor

As well all known, the reproducibility of an electrochemical immunosensor is a key factor for practical applications. The reproducibility was investigated by assaying three different concentration levels (1.0 ng/mL, 10 ng/mL, and 50 ng/mL) for five immunosensor arrays that were made in the same batch. As shown in Fig. 6A, experimental results revealed the relative standard deviation (RSD) of the measurements were 2.08%, 3.63% and 2.37%. The acceptable reproducibility of the proposed immunosensor was ascribed to synergetic effect that occurs at Au@PDA and Au@Pt DNs/NG/Cu^{2+}.

The selectivity of the immunosensor was further investigated by detecting the current response of five working electrodes. Selective determination of target analyses plays an important role in analyzing biological samples. The effect of possible inhibitors that might interfere with the response of immunosensor was investigated. Interference studies were performed using prostate specific antigen (PSA), immunoglobulin G (IgG), BSA, hepatitis B surface antigen (HBs) and hepatitis B e (HBe). The 1.0 ng/mL of CEA solution containing 100 ng/mL of interfering

substances was measured by the immunosensor and the results were shown in Fig. 6B. The current variation due to the interfering substances was less than 5.0% of that without interferences, indicating that the selectivity of the immunosensor was acceptable.

Stability is a vital factor to assess the performance of the developed immunosensor. As illustrated in Fig. 6C, when the immunosensor was prepared and not in use, it was stored in a refrigerator at 4 °C. The current response of the as-prepared immunosensor decreased 3.9% after 6-day storage. Three weeks later, the current response of the immunosensor was decreased to about 89% of its initial value. The slow decrease in the current response indicated that the immunosensor possessed the well-characterized of good stability. And the results compared with different immunosensors were summarized in Table S3, which also illustrated that the designed immunosensor had a better stability, and further confirmed that the proposed nanomaterials exhibited a good stability in the CEA detection and held a promising potential for practical application.

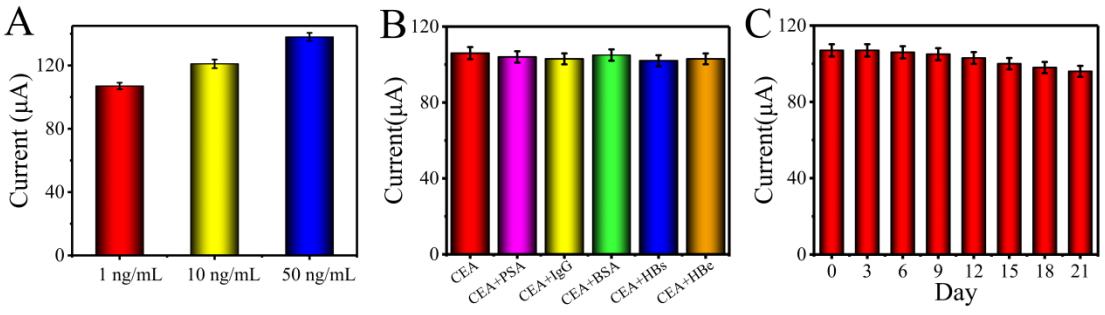

Fig. 6. (A) Electrocatalytic current responses of the immunosensor fabricated on three

groups of electrodes for the detection of 1.0 ng/mL, 10 ng/mL, 50 ng/mL CEA. (B) Amperometric response of the immunosensor to 1.0 ng/mL CEA, 1.0 ng/mL CEA + 100 ng/mL PSA, 1.0 ng/mL CEA + 100 ng/mL IgG, 1.0 ng/mL CEA + 100 ng/mL BSA, 1.0 ng/mL CEA + 100 ng/mL HBs, 1.0 ng/mL CEA + 100 ng/mL HBe. (C) The stability studies of the CEA immunosensor. Error bar = RSD (n = 5).

3.8. Real sample analysis

To test the applicability and reliability of the proposed immunosensor to be applied for practical analysis, the immunosensor was used to analyze CEA in human serum by the standard addition method (Bo and Kowalski, 1979), the results were presented in Table S4. As shown in Table S4, the recovery was from 98.24% to 102.30% with the RSD values ranging between 2.0% to 5.5%, indicating that the immunosensor had good sensitivity and accuracy. The results obtained by this method compared with enzyme-linked immunosorbent assay (ELISA), the data were shown in Table S4, the recovery was from 97.71% to 101.35% and RSD was from 2.4% to 7.0%. Furthermore, the relative errors between the two methods were less than 2.3% for detection of CEA. The results showed a good correlation between these two analytical methods, indicating this immunosensor showed acceptable feasibility to detect CEA in human serum. In addition, the validity of the immunosensor was evaluated by comparing with other methods. As shown in Table S5, satisfactory results were achieved, which also

indicated that the proposed procedure was sensitive and accurate enough for practical applications.

4. Conclusions

In conclusion, we developed a new electrochemical immunosensor based on Au@Pt DNs/NG/Cu^{2+} with enhanced peroxidase-like properties as labels and Au@PDA as substances for the ultrasensitive detection of CEA with diagnostic efficiency and accuracy. The Au@PDA modified GCE was found to exhibit good conductivity and adhesivity. Furthermore, Au@Pt DNs/NG/Cu^{2+} with larger surface area and better electrochemical properties, the electrochemical signal was greatly amplified and resulted in good analytical performance. Consequently, a linear correlation between the current and analytic concentration over a desirable linear range and the lower detection limit may readily be inferred. More importantly, the electrochemical immunosensor was also found to exhibit acceptable reproducibility, good selectivity and sensitivity for detection of CEA. What's more, when the immunosensor was used to the analysis of CEA in human serum, satisfactory recoveries were obtained. The proposed method provides a promising alternative for the determination of CEA in real samples.

Acknowledgments

This study was financially supported by the National Natural Science Foundation of China (Nos. 21575079; 21575050 and 31071538).

All of the authors express their deep thanks.

References

Barton, M.K., 2014. Ca A Cancer Journal for Clinicians 64, 365-366.

Bo, E.H.S., Kowalski, B.R., 1979. Analytical Chemistry 51, 1031-1038.

Chen, Z., Liang, R., Guo, X., Liang, J., Deng, Q., Li, M., An, T., Liu, T., Wu, Y., 2016. Biosensors & Bioelectronics 91, 60-65.

Fan, F.R., Liu, D.Y., Wu, Y.F., Duan, S., Xie, Z.X., Jiang, Z.Y., Tian, Z.Q., 2008. Journal of the American Chemical Society 130, 6949-6951.

Fan, H., Li, Y., Wu, D., Ma, H., Mao, K., Fan, D., Du, B., Li, H., Wei, Q., 2012. Analytica Chimica Acta 711, 24-28.

Frens, G., 1973. Macmillan company 241, 20-22.

Guo, C., Su, F., Song, Y., Hu, B., Wang, M., He, L., Peng, D., Zhang, Z., 2017. Acs Applied Materials & Interfaces 179, 71-81.

Hasanzadeh, M., Shadjou, N., Lin, Y., Guardia, M.D.L., 2016. Trac Trends in Analytical Chemistry 86, 185-205.

Jiang, L., Jian, H., Li, F., Jian, G., Li, Y., Dong, Y., Qin, W., 2015. Electrochimica Acta 160, 7-14.

Li, F., Han, J., Jiang, L., Wang, Y., Li, Y., Dong, Y., Wei, Q., 2015. Biosensors & Bioelectronics 68, 626-632.

Li, N.L., Jia, L.P., Ma, R.N., Jia, W.L., Lu, Y.Y., Shi, S.S., Wang, H.S., 2016. Biosensors & Bioelectronics 89, 453-460.

Li, W., Yuan, R., Chai, Y., Chen, S., 2010. Biosensors & Bioelectronics

25, 2548-2552.

Li, Y., He, J., Chen, J., Niu, Y., Zhao, Y., Zhang, Y., Yu, C., 2017. Biosensors & Bioelectronics 101, 7-13.

Lim, B., Lu, X., Jiang, M., Camargo, P.H., Cho, E.C., Lee, E.P., Xia, Y., 2008. Nano Letters 8, 4043-4047.

Liu, P.Y., Yue, H., Tian, W., Chen, Y., Li, F., 2009. Analytical Letters 42, 45-57.

Liu, T.D., Xu, L.Y., Shao, G.F., Tu, N.N., Tao, J.P., Wen, Y.H., 2016. Journal of Alloys & Compounds 663, 466-473.

Lv, H., Li, Y., Zhang, X., Gao, Z., Feng, J., Wang, P., Dong, Y., 2017. Analytica Chimica Acta 1007, 61-70.

Sheng, K., Liu, W., Xu, L., Jiang, Y., Zhang, X., Dong, B., Lu, G., Song, H., 2017. Sensors & Actuators B Chemical 254, 660-668.

Wang, L., Yamauchi, Y., 2010. Chemistry, an Asian journal 5, 2493-2498.

Wang, L., Yamauchi, Y., 2011. Chemistry of Materials 23, 2457-2465.

Wang, R., Liu, W.D., Wang, A.J., Xue, Y., Wu, L., Feng, J.J., 2017a. Biosensors & Bioelectronics 99, 458-463.

Wang, R., Ma, H., Zhang, Y., Wang, Q., Yang, Z., Du, B., Wu, D., Wei, Q., 2017b. Biosensors & Bioelectronics 96, 345-350.

Wang, Y., Shao, Y., Matson, D.W., Li, J., Lin, Y., 2010. Acs Nano 4, 1790-1798.

Wen, W., Yan, X., Zhu, C., Du, D., Lin, Y., 2016. Analytical Chemistry

494, 10-15.

Sun, Y., Xia, Y., 2002. Science (New York, N.Y.) 298, 2176-2179.

Yadav, R., Dixit, C.K., 2017. Journal of Science Advanced Materials & Devices 2, 141-149.

Yang, Z., Cao, Y., Li, J., Jian, Z., Zhang, Y., Hu, X., 2015. Analytica Chimica Acta 871, 35-42.

Yang, Z., Lu, M., Li, J., Tan, Z., Dai, H., Jiao, X., Hu, X., 2016. Biosensors & Bioelectronics 89, 558-564.

Zhang, W., Li, L., Hai, J., Meng, T., Zhang, J., Feng, X., 2011. Chinese Science Bulletin 56, 3583-3589.

Zbar, A.P., Lemoine, N.R., Wadhwa, M., Thomas, H., Snary, D., Kmiot, W.A., 1998. British Journal of Cancer 77, 683-693.

Zhang, S., Shen, Y., Shen, G., Wang, S., Shen, G., Yu, R., 2016. Analytical Biochemistry 494, 10-15.

Zhang, X., Li, Y., Lv, H., Feng, J., Gao, Z., Wang, P., Dong, Y., Liu, Q., Zhao, Z., 2018. Biosensors & Bioelectronics 106, 142-148.

Highlights

- Sandwich-type electrochemical immunosensor for the detection of CEA was constructed.
- Au NPs functionalized PDA as transducing materials to enhance the conductivity.
- Au@Pt DNs/NG/Cu^{2+} with enhanced peroxidase-like properties as labels was synthesized.
- The immunosensor exhibited a low detection limit of 0.167pg/mL for CEA.